applied sciences

MDPI

Review

Bone: An Outstanding Composite Material

Natacha Rosa [1,2,*], Marcelo F. S. F. Moura [1], Susana Olhero [3], Ricardo Simoes [4,5], Fernão D. Magalhães [6], António Torres Marques [1], João P. S. Ferreira [1,2], Ana Rita Reis [1,2], Mariana Carvalho [1,2] and Marco Parente [1,2]

1 DEMec, Faculty of Engineering, University of Porto, Rua Roberto Frias, 4200-465 Porto, Portugal; mfmoura@fe.up.pt (M.F.S.F.M.); marques@fe.up.pt (A.T.M.); j.ferreira@fe.up.pt (J.P.S.F.); arreis@inegi.up.pt (A.R.R.); up201605417@fe.up.pt (M.C.); mparente@fe.up.pt (M.P.)
2 INEGI—Institute of Science and Innovation in Mechanical and Industrial Engineering, 4200-465 Porto, Portugal
3 Department of Materials and Ceramic Engineering (DEMaC), CICECO-Aveiro Institute of Materials, University of Aveiro, 3810-193 Aveiro, Portugal; susana.olhero@ua.pt
4 Polytechnique Institute of Cávado and Ave, School of Technology, Campus do IPCA, 4750-810 Barcelos, Portugal; rsimoes@ipca.pt
5 Institute for Polymers and Composites IPC/I3N, University of Minho, Campus de Azurém, 4800-058 Guimarães, Portugal
6 LEPABE—Faculdade de Engenharia da Universidade do Porto, Rua Roberto Frias, 4200-465 Porto, Portugal; fdmagalh@fe.up.pt
* Correspondence: natacharosa22@gmail.com

Abstract: Bone is an outstanding, well-designed composite. It is constituted by a multi-level structure wherein its properties and behavior are dependent on its composition and structural organization at different length scales. The combination of unique mechanical properties with adaptive and self-healing abilities makes bone an innovative model for the future design of synthetic biomimetic composites with improved performance in bone repair and regeneration. However, the relation between structure and properties in bone is very complex. In this review article, we intend to describe the hierarchical organization of bone on progressively greater scales and present the basic concepts that are fundamental to understanding the arrangement-based mechanical properties at each length scale and their influence on bone's overall structural behavior. The need for a better understanding of bone's intricate composite structure is also highlighted.

Keywords: biomechanics; biomedical engineering; architecture; bone tissue; composite

Citation: Rosa, N.; Moura, M.F.S.F.; Olhero, S.; Simoes, R.; Magalhães, F.D.; Marques, A.T.; Ferreira, J.P.S.; Reis, A.R.; Carvalho, M.; Parente, M. Bone: An Outstanding Composite Material. *Appl. Sci.* **2022**, *12*, 3381. https://doi.org/10.3390/app12073381

Academic Editor: Claudio Belvedere

Received: 15 February 2022
Accepted: 23 March 2022
Published: 26 March 2022

1. Introduction

Bone, the main component of the skeleton system, is a crucial constituent of the complex and coordinated multipart "machine" that is the human body [1]. Besides its biological purpose as a mineral reservoir (e.g., for calcium, phosphate, and magnesium), in calcemia regulation, and its role as the host site for hematopoietic tissue (e.g., bone marrow), bone fulfills a range of demanding mechanical functions. It is responsible for internal organ (e.g., the brain) and tissue (e.g., bone marrow) protection and also body support and motion through muscles' attachment to its surface [2,3]. The mechanical behavior of bone is determined by its composition and structural organization at different length scales, which in turn is established, to a certain extent, by its mechanical environment [4,5]. An increasing interest in understanding the principles that determine the multi-level hierarchical properties of biological composites has been stated [6]. These living materials present a combination of mechanical properties, not yet attained by synthetic composites with similar configurations [7,8]. Hence, the linking between structure and properties in bone, combined with its adaptive ability, make it an exceptional composite with high interest in the fields of engineering and material design. This review article focuses on the human tibia, aiming to

describe the hierarchical organization of bone on progressively greater scales and hopefully contribute to a better understanding of how the arrangement-based mechanical properties in each level influence the bone whole-structure biomechanical behavior.

2. Nanostructure

Bone is composed of a weight fraction range of 65–70% inorganic component, 18–25% organic, and 10−12% water, whereas on a volume fraction range, the proportions for each component are between 33 and 43%, 32 and 44%, and 15 and 25%, respectively [9]. It should be noted that this ratio can vary depending on the age and health conditions of the human being [10].

The organic phase of bone composite consists primarily of type I collagen (90% by weight), some other minor collagen types (III and VI), and a variety of non-collagenous proteins such as laminin, fibronectin, vitronectin, osteocalcin, osteonectin, osteopontin, and bone sialoprotein [11]. The basic structural unit of collagen is called tropocollagen (see Figure 1), which is a very rigid linear molecule with a diameter and length of 1.1 nm and 300 nm, respectively [12]. This molecule possesses a rearranged, right-handed, triple-helix structure formed by polypeptide chains with a highly repetitive amino acid sequence, glycine-X-Y, where glycine is being used in every third residue and X is often proline and Y is frequently hydroxyproline [13,14]. This frequent occurrence of proline and hydroxyproline stabilizes the polypeptide strands (e.g., through interchain hydrogen bonds) and limits rotations, leading to its tightly packed triple-helical form [15]. The triple-helix structures are associated with microfibrils, where five tropocollagens are assembled in parallel (D-period) [13]. At the next level of the hierarchy, the tropocollagen molecules congregate into fibrils by being covalently cross-linked at their tips and their axial staggering, forming overlap zones and gaps with a specific periodicity of approximately 67 nm [12,15].

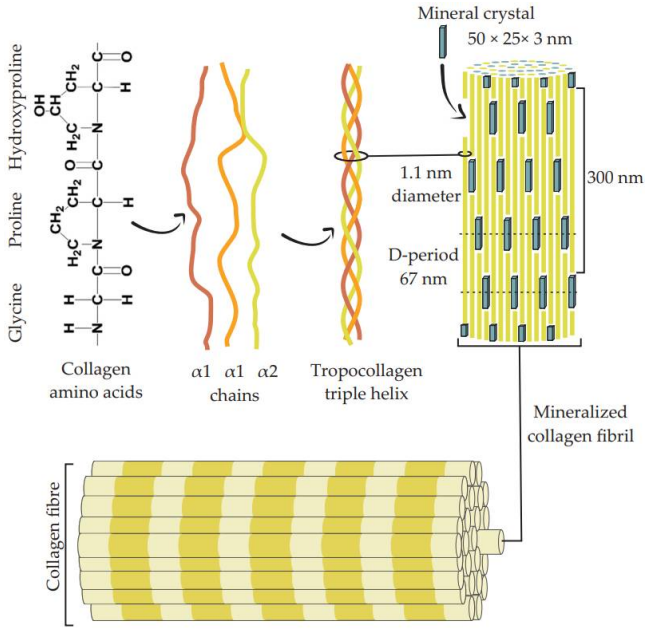

Figure 1. Representation of the collagen fibers' structural organization. The type I collagen major amino acid components Gly-Pro-HyPro constituting the α chains are self-assembled in a triple-helix, tropocollagen structure. Stacks of mineral crystals lie between the congregated tropocollagen molecules to form mineralized collagen fibrils with a characteristic D-period. These fibril molecules are then packaged to form collagen fibers [16–19].

The inorganic phase of bone is a ceramic crystalline-type mineral, as an impure form of naturally occurring calcium phosphate, most often referred to as biological non-stoichiometric hydroxyapatite. Bone hydroxyapatite is not pure hydroxyapatite, because the tiny apatite crystals contain impurities such as potassium, magnesium, strontium,

sodium (in place of the calcium ions), carbonate (4 to 6% of the phosphate groups are replaced by carbonate groups), and chloride or fluoride (in place of the hydroxyl ions). These impurities reduce the crystallinity of the apatite and consequently alter some properties, such as solubility, which is crucial for mineral homeostasis and bone adaptation. There is a long ongoing debate about the nature of the mineral particle shape—needles versus platelets [20–22]. More recently, the existence of mineral particles with a fractal aggregate shape was also discovered [23].

At the submicron scale, bone is composed of building blocks of mainly type I collagen, mineral crystals, water, and non-collagenous proteins [24]. The organic and inorganic components of bone blend together to generate mineralized collagen fibrils, as demonstrated in Figure 1. The mineral component in bone occurs as stacks of thin polycrystalline sheets, which surround and lie between the collagen fibrils [12]. The collagen–mineral system is arranged in parallel arrays within thin sheets called lamellae. As stated previously, the organization of the lamellae differs between cortical and trabecular bone. As identified by Fratzl et al. [25], the lamellae are assembled in a "rotated plywood-like fashion" in cortical bone. In cancellous bone and according to Chen et al. [26], these structures are strongly fused, forming a sheet-like structure.

The mechanical properties of the organic and inorganic phases together with their hierarchical arrangement confer bone features that determine its characteristic strength and toughness [27]. The mineral content predominantly contributes to bone stiffness and strength. Therefore, when the organic collagen in bone is removed—by heat or leach—mature bone becomes brittle [25,26,28]. Based on a computational study [27] where nanoindentation data were considered, single hydroxyapatite crystals demonstrated stiffness values of 150 GPa and 143 GPa in the [0001] and [1010] direction, respectively. In a more recent study, Pang et al. [29] identified the presence of an organic substance binding the mineral components together, and the authors believe that it contributes to the strength, stiffness, and energy absorption of bone under compression. In a thorough study [24], Wang and Ural demonstrated that the increase in the elastic modulus, ultimate strength, and fracture energy of the mineralized collagen fibrils networks was significantly influenced by both the increased uniformity of mineral distribution and stronger interactions between the components and was modestly influenced by the rise in total volume fraction of minerals. This study also concluded that the mineral distribution had the most drastic influence on the elastic modulus compared to the ultimate strength and fracture energy. However, bone strength does not depend solely on bone mineral distribution, but also on the quality and material properties of the organic component where collagen cross-links play an important role in the reinforcement of bone strength [30]. Significant determinants of the functional integrity of the organic phase are the degree and nature of enzymatic lysyl oxidase-mediated collagen crosslinks and the negative effects of non-enzymatic glycation-induced collagen crosslink (the production of advanced glycation end-products such as pentosidine), which can be considered in a competitive relationship with enzyme-derived cross-linking [31,32]. Enzymatic cross-linking density has been related to governing post-yield and large-scale mechanics, and cross-link strength governs failure strain, hence improving fracture toughness, bone strength, and stiffness [33–35]. Meanwhile, non-enzymatic cross-linking is related to the prevention of energy absorption by microdamage formations, reducing bone toughness and ultimate strain [36,37] and accelerating brittle fracturing [38,39].

Mineralized collagen fibrils are embedded in an extrafibrillar matrix that consists of water, mineral, and non-collagenous proteins [37]. A recent study [9] used positron annihilation lifetime spectroscopy (PALS), a technique sensible to voids/pores at the nanometer and subnanometer scale, to observe these structures. It was noticed that water mainly occupies the regions in intercollagen molecular spaces, terminal segments (D-spacing) within collagen microfibrils, and interface spacing between collagen and mineral structures. Water was also identified as being loosely bound to the surfaces of collagen fibrils [12]. The bone water content is an essential component since it confers much of bone's unique strength and resilience by stress reduction during dynamic loading [40,41].

Hence, removing bound water in the bone matrix makes bone stiffer, stronger, but more brittle at different length scales, because dry collagen loses its deformation and energy absorption capacity [42]. As stated by Leo et al. [13], the lack of collagen external water promotes the formation not only of new inter-tropocollagen hydrogen bonds but also of intra-tropocollagen ones, which cause the microfibril gain of compactness and tubularity. These molecular and supramolecular changes are responsible for the generation of very large stresses up to 100 MPa when the collagen undergoes complete dehydration [43]. Bone mechanical properties are not only intimately linked to its nanostructure composition but also to its organization, where further study and profound understanding are still needed.

3. Microstructure

There are two types of bone tissues: primary or woven bone, present in newly developed immature bone at fracture site callus, and lamellar bone, which is the more mature form of bone, found in the adult human skeleton. In cortical bone, lamellar bone can be found as extended parallel arrays called circumferential lamellae and also as smaller lamellae cylindrical structure arrangements, called osteon (or the Haversian system). Each osteon consists of about 10 to 30 lamellae arranged in concentric cylinders built up around the neurovascular channel, called the Haversian canal (see Figure 2). The outer surface of the osteon constituted by a thin layer of calcified mucopolysaccharides, the cement line, is the weaker cracking path, leading to crack deflection. Cancellous bone consists primarily of lamellae, arranged in a less organized lattice-like network of matrix spikes, called trabeculae, to form a network of rods and plates, which on average have a thickness in the range of 100–200 μm. Trabeculae are interspersed with large bone spaces (in the order of 500 to 1500 μm) filled with bone marrow [44–46]. Unlike the elastic properties, the post-yield properties and failure mechanisms of bone under compression differ significantly at the two length scales. Schwiedrzik et al. [47] demonstrated that isolated bone lamellae show high strength and ductility but no damage and fail mostly by the development of shear planes, while the response of macroscopic specimens containing numerous osteons is quasi-brittle with low strength and ductility, presenting substantial damage and longitudinal cracks.

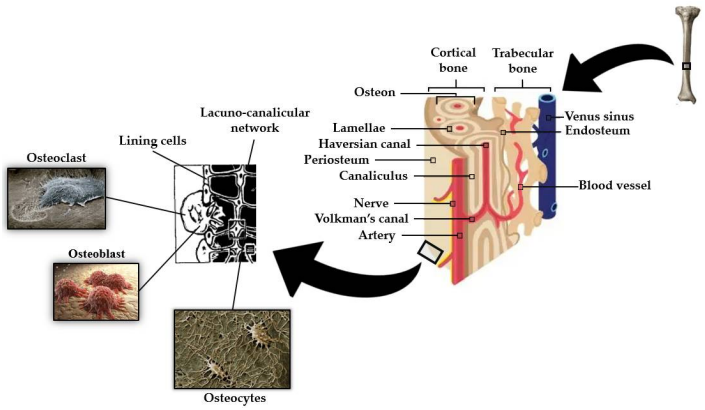

Figure 2. Diagram showing tibia diaphysis bone microscopic hierarchical organization and its main cellular population [48–52] With permission from the International Osteoporosis Foundation.

An outstanding feature of bone is the fact that its mass is maintained by and adapted to mechanical strain [5]. This mechanotransduction process is a well-orchestrated cellular event regulated by complex interactions between the various cell types found in bone, primarily osteoblasts, osteoclasts, and osteocytes (see Figure 2) [53].

Osteocytes have become generally accepted as the mechanosensory cells within the bone [5]. The mechanosensation and mechanotransduction mechanisms in osteocytes arise from their unique stellate shape and interconnected architecture. An osteocyte is made up of an ellipsoid cell body that occupies a fluid-filled space within its lacunae. Osteocytes are interconnected by many long dendritic processes that pass through a network of small

channels called canaliculi (as can be seen in Figure 2) [54,55]. The process of converting external mechanical forces into biochemical responses, known as mechanotransduction [5], includes the response of the osteocyte to the cell direct mechanical deformation/strain as a consequence of bone matrix strain [56], to shear stress due to load-induced fluid flow [57], to electric fields caused by stress-generated streaming potentials [58], and to hydrostatic pressure [59]. Recent mechano-regulatory in vitro and in silico bone tissue engineering experiments [60] point towards the determinant influence of low shear strain and fluid velocity in bone adaptive response and cell differentiation. Despite the mechanism of stimuli perception in osteocytes not being fully understood, both cell bodies (e.g., osteocytes plasma membrane disruptions) [61] and dendritic processes [62,63] have been proven to perceive mechanical forces applied to the bone. Kola et al. [55] demonstrated that lacunar strain value increased as lacunae size increased, with the highest strain magnification ratio observed for horizontally aligned lacunae. The authors also demonstrated the influence of the perilacunar region modulus in the strain magnification generated at the lacuna. Variations in lacunar morphology such as an increase in lacuna sphericity cause changes in the mechanical environment of osteocytes, in particular a decrease in maximum effective local strains [64].

In addition to their hosting-site and sensorial stimuli mechanisms for osteocytes, lacunae have a structural role in the local mechanical properties and fracture behavior of the bone matrix. In a finite element study developed by Hamed and Jasiuk [65], the apparent elastic modulus of the bone matrix was lowered by the existence of osteocyte lacunae. Kaya et al. [66] verified that bone elastic modulus changes were related to cumulative increases in void volume in lacunae and canaliculi, which were induced by rat models' lactation and recovery stages. More recently, Sang et al. [67] demonstrated a significant linear relation between the physiological range of osteocyte lacunar porosity area, density, size, and orientation and the elastic modulus and ultimate strength of the bone matrix in virgin and lactation rats. The influence of osteocyte lacunae structure on crack initiation and propagation has also been studied. Lacunae voids create bands of stress concentrations as a result of high local strains around osteocytes, providing a site for crack nucleation [68]. According to Josephson et al. [69], despite the number of lacunae damage initiation sites and the rate of crack growth, perilacunar regions can delay or prevent the emergence and growth of microcracks. In the study developed by Sang et al. [67], osteocyte lacunae demonstrated a guiding effect on the cracks, i.e., attracted a nearby crack due to stress concentrations near lacunar boundaries. The authors also inferred that a reduced density of osteocyte lacunae may also lead to regions where the crack may grow more easily, which may have an adverse impact on bone fragility fractures. In this study, there was no relation between the energy dissipated during damage and crack formation, a measure of fracture resistance, and the osteocyte lacunae structural parameters.

After sensing mechanical loads applied to the bone, osteocytes react by controlling osteoblast and osteoclast activities through cell-to-cell communication and via secreted factors [70]. Osteocytes connect to cells on the bone surface and the vasculature by many long dendritic cytoplasmic processes ranging from 40 to 100 per cell [71]. Osteocytes and osteoblasts communicate with one another through gap junctions present on the tips of the cell processes. These are bidirectionally transmembranar channels that connect the cytoplasm of two adjacent cells and regulate the passage of molecules less than 1 kDa [71].

Osteoblasts are secretory cells, responsible for the formation of the pre-mineralized bone matrix, called osteoid, predominantly comprising bony matrix proteins such as type I collagen and trace quantities of type V collagen, and also other non-collagenous proteins such as osteopontin, osteocalcin, osteonectin, osteoprotegerin, bone morphogenetic proteins, and glycoproteins. The mineralization process of osteoid involves the supersaturation of extracellular fluids at local zones and increased osteoblastic alkaline phosphatase activity, which raises local calcium and phosphate concentrations. Osteoblasts produce osteocalcin protein, which binds calcium and further concentrates local calcium levels [40,72–75].

During the process of bone formation, some osteoblasts, involved in the production of bone matrix, become embedded in that matrix. The fundamental question of how osteoblasts are buried remains largely unanswered. The matrix around a newly incorporated cell is not yet calcified (osteoid) but gradually calcifies as the formation front moves away because of continuing osteoblastic activity. Osteoid osteocytes still possess many features of the original osteoblast, and their major functions are to simultaneously: (i) regulate mineralization because they are not as active as osteoblasts in the generation of a mineralized matrix, (ii) reduce the number of organelles and cytoplasmic volume, and (iii) gain the long connective slender cell processes [40,76,77].

Osteoclasts are irregularly shaped giant cells (15 to 20 μm or more) that originate from monocytes and macrophages (two types of white blood cells). They are specialized in the local removal of bone during growth and during the remodeling of osteons and bone surfaces. These cells are found in depressions called Howship's lacunae or resorption bays. For bone resorption to occur, osteoclasts have an interface known as the "ruffled brush" border, formed by a highly enfolded plasma membrane, which increases the surface area. The "ruffled brush" border is surrounded by a clear zone, as well as a well-defined zone of actin filaments responsible for bone resorption. Osteoclasts bind to bone surfaces via anchoring proteins such as integrins and create a seal and lower the pH by releasing protons (e.g., hydrogen ions via carbonic anhydrase) and by expressing acid hydrolases (e.g., tartrate-resistant acid phosphate). This environment is suited to increase the solubility of hydroxyapatite crystals as well as destroy the organic matrix with lysosomal (cathepsin K) and non-lysosomal (collagenase) enzymes. The osteoclastic bone resorption is inhibited by calcitonin and interleukin-10 and stimulated by osteoblast-derived signals, cytokines from cells, including macrophages and lymphocytes (e.g., interleukin-1), and blood-circulating factors (e.g., parathyroid hormone) (see Figure 3) [40,72].

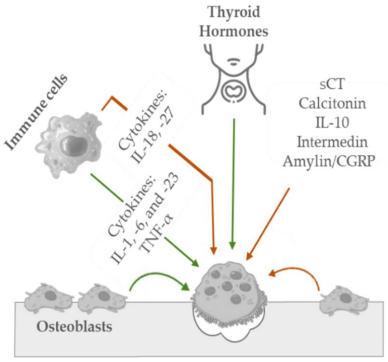

Figure 3. Schematic representation of the key mediators in osteoclastic bone inhibition (orange arrow) and stimulation (green arrow) mechanisms.

Hence, throughout life and in response to mechanical and physiological stimuli, bones suffer growth and processes of shaping and reshaping by independent actions of osteoblasts and osteoclasts (a process known as bone modeling) and are subjected to continuous and dynamic equilibrium (bone resorption and formation), responsible for preserving its functional integrity (a process known as bone remodeling) [53,70]. Despite the complexity of the rules that govern the effects of bone mechanical loading on cells and tissue differentiation, growth, adaptation, and maintenance, research efforts are being applied to try to describe and understand these complex phenomena through the challenging task of developing microscale mechanobiology computational models. Numerical methods, such as finite element simulation, are being considered for the development of these models by integrating the contributions of applied external mechanical loads, cellular activities, and cellular nutrients, such as oxygen and glucose supply [78], the incorporation of biochemical osteocyte feedback [79], angiogenesis [80], and the autocrine and paracrine signaling pathways of bone cells [81]. Once the mechanisms of mechanically regulated

bone response are better understood, physiological conditions and pharmacological agents may be developed to promote better and faster bone tissue repair and formation [82].

4. Macrostructure

At the highest hierarchical level, long bones are constituted by the cortical bone (also known as compact bone) and trabecular bone (also known as cancellous or spongy bone). Although they have similar compositions, the different structure arrangements and porosity levels grant unique mechanical properties and functions to each structure. The cortical bone is a compact structure with porosity ranging from 5 to 30%. For example, adult human femoral cortical bone porosity can vary from as low as 5% at the age of 20 and up to 30% above the age of 80 [21,28,83]. The trabecular bone has a spongier, lightweight, and honeycomb structure with porosity values of approximately 70% with higher values in some cases, such as the elderly spine, where 95% porosity is reached [25,28,84–87]. In the tibia, the diaphysis is the central portion of the bone and is characterized by the lowest width dimension. It is responsible for the load transmission between the two extremities (epiphysis and metaphysis at both ends) and has stiff cortical bone walls [88,89]. The tibia epiphysis is characterized by bulk trabecular bone (containing vessels, nerves, and bone marrow) coated with a thin layer of cortical tissue [90,91]. Cortical bone carries a considerable share of the total skeleton load. As demonstrated in a study developed by Papini et al. [92], there was a negligible variation in axial and torsional stiffness values prediction by the finite element model if only the cortical bone was considered in the simulation. This was justified by the considerable difference between the Young's modulus of the cortical (10–40 GPa) [93–98] and the trabecular bone (0.05–0.5 GPa) [93]. This demonstrated that it is the cortical rather than the spongy bone that is mainly responsible for most of the weight support. In the epiphyseal and metaphyseal regions, where cortical bone thickness is reduced, weight-bearing is achieved by stress reduction with the increase in surface area and load diversion. Stress varies inversely with the loaded cross-sectional area, which indicates that stress on the joint will be reduced with the increase in the surface area. The spongy nature of the ends of the tibia segment confers weight-bearing distribution in local trabeculae, hence it dissipates loads and absorbs energy. As the weight-bearing is transferred from the metaphysis to the diaphysis, it becomes more dependent on the cortical layer, which, in turn, becomes thicker and more resistant [4,99]. It is important to highlight that the expansion of the bone ends is limited by the reduction in the joint friction to a minimum value (e.g., reduced weight of the bone ends will reduce the normal reaction force, while the reduced length of the radius of curvature will reduce the magnitude of the moment of friction). Considering the interesting case of the tibia as a load-bearing bone example, it articulates proximally at the knee joint and distally at the ankle, being the weight-bearing bone of the leg [100]. The body weight-bearing load on the tibia plateau is assumed to be divided into a central concentric and a medial and lateral eccentric knee contact force (split around 60 and 40% on the medial and lateral condyles, respectively). The higher loads on the medial side relative to the lateral side (see Table 1) is consistent with the fact that the medial side of the tibia has a larger condyle, and the bone is also denser and stronger than that of the lateral side. Hence, there is a balance in the bending stress generated between the condyles. According to Munford et al. [101], by studying the distribution of cancellous bone mechanical properties in the proximal tibia, they determined that average apparent modulus and strength were 1.7 and 3 times higher in the axial direction compared to the transverse directions, respectively. They also verified that in the dominant axial direction, the bone was 1.3 times stiffer in the medial condyle than the lateral condyle. Although only a few important features of the weight-bearing mechanism of the proximal tibia were presented here, the contact mechanism between the femoral and tibial articular surfaces are complex and consist of many unique features, and its biomechanics is not still fully understood [90,97,102,103]. In the case of the ankle, it is expanded to a lesser extent when compared to the upper joint. This occurs since the load of body weight that is transmitted through the lower leg divides itself into two components, which resolve into vertical and

horizontal force when it reaches the talus trochlea. The horizontal force will stretch the plantar ligaments and muscles, and the vertical load will be lesser than the actual load transmitted along the long bone [90]. During daily activities, such as normal level walking, the tibiofemoral joint experiences high compressive loads around 3 times the body weight (normally expressed as ×BW), i.e., 2058 N if a 70 kg adult was considered. However, more strenuous activities such as squats can raise the load values for up to 7.3 times the body weight, i.e., 5008 N if the same body weight was considered (see Table 1).

Table 1. Peak tibiofemoral joint compressive forces during several daily activities and expressed as times the bodyweight.

Activity		Knee Contact Force (×BW)			Study [1]	Reference
		Medial		Lateral		
		1st Peak	2nd Peak			
Level walking			3.2		In vivo	[104]
			2.8		Simulation	[105]
		<2.4	2.4	1	In vivo	[103]
		2.2–2.5	2.37–2.51	Similar	In vivo	[106]
			2.8		In vivo	[107]
			3.3		Simulation	[108]
			3.1		Simulation	[109]
			4.0		In vivo	[110]
			2.8		In vivo	[111]
		2		1.5	In vivo	[112]
		1.3–1.5	1.3–1.5	0.8–1.15	In vivo	[113]
			2.8		Simulation	[105]
			3.3		Simulation	[108]
			2.9		In vivo	[114]
Stair	Ascending	2.28–2.5	2.28	-	In vivo	[106]
			2.8		In vivo	[107]
			5.3		In vivo	[110]
			2.9		In vivo	[111]
			5.4		Simulation	[109]
		2.63–2.81	2.8	-	In vivo	[106]
	Descending		3.1		In vivo	[107]
			3.3		In vivo	[111]
Rising from chair		2.09	-	-	In vivo	[106]
			2.6		In vivo	[111]
			3.38–7.89		In vivo	[115]
Jogging			3.6		In vivo	[107]
Squats			7.3		In vivo	[110]
			6.3		In vivo	[116]
			4.7–5.6		In vivo	[117]

[1] The correct determination of the load applied to the tibia bone would be through the measurement of the forces in in vivo, which is limited and not feasible in healthy subjects or patients with pathology not requiring a total knee replacement. Therefore, in most studies where physiological data were acquired, "kinesiological techniques", such as high-speed time camera, force platform, and electromyographic recorder, were used. The results obtained were considered in this article as being in vivo or as close as possible to in vivo data.

5. Mechanical Behavior

The ordered lamellar structure confers bone tissue an anisotropic behavior with direction-dependent material properties. Cortical bone strength, yield stress, and Young's modulus have higher values in compression than in tension along the direction aligned with the diaphyseal axis rather than transversely. In the latter, it is weaker in tension than in compression. Although the microstructural mechanism that causes the differences in yield and post-yield behavior is still not completely understood, it is generally accepted that when the cortical bone is loaded past the yield point, it accumulates permanent damage within the bone tissue. Such phenomena may also occur even when the cortical bone is unloaded near the yield point. After the yield point is exceeded, the reloading modulus presents a lower value. This is associated with the cortical bone degradation characteristics. The tissue microstructure deterioration appears as "microdamage" accumulation as a result of static or cyclic loading. In such a case, cortical bone has greater resistance in compression than in tension.

Damage initiation and growth should be analyzed using fracture mechanics concepts. The objective is to determine fracture toughness (the mechanical property that describes the bone resistance to crack initiation and propagation) under different loading modes, i.e., opening (mode I), shear sliding (mode II), and shear tearing (mode III). These loading modes, and a combination of them, occur frequently during normal daily activities, such as walking or running, for example. Aiming to perform bone fracture characterization, several different tests have been used. The compact tension [118], single-edge notched beam [119] and double cantilever beam [120] tests have been employed for fracture characterization of bone under mode I loading. Under mode II loading, Norman et al. [121] proposed the compact shear test, and Dourado et al. [122] used the end notched flexure test. The mixed-mode I + II loading fracture characterization of bone has been studied considering the asymmetric four-point bending test using single-edge notched specimens [123], the single-leg bending test [124], and the mixed-mode bending test [125]. The initial methods utilized to study the fracture risks of bone under different conditions were based on linear elastic fracture mechanics concepts [118,126]. However, the bone complex microstructure and composition gives rise to the development of a non-negligible fracture process zone, which is the region close to the crack tip, where several phenomena such as microcracking, crack deviation, and fiber bridging occur. In this context, non-linear fracture mechanics-based methods, such as cohesive zone modeling, are more appropriate [120,127].

Another important characteristic of cortical bone is its viscoelasticity, although only moderately. This means that the stress developed within the bone, and consequently its stiffness and strength, are dependent on the rate at which bone is strained. A six order of magnitude increase in strain rate will only change the Young's modulus by a factor of two and strength by a factor of three. The positive effect of this property is accentuated during impact loading (e.g., high energy impact), where strength can increase by a factor of three [21,88,128–130].

In cancellous bone, the mechanical properties of the constituents and trabecular architecture are the main factors determining its mechanical performance [131]. In trabecular bone, the strength is highest in compression rather than in tension and lowest in shear, which is likewise in cortical bone. Oppositely to the fairly linear behavior verified at low stress values in cortical bone stress–strain curve, in trabecular bone, such a performance is absent, and there is no clear linear region. The nonlinearity is even present at low stress levels. An interesting property of the trabecular bone is that it can absorb substantial energy on mechanical failure. Although it yields in compression at strains between 0.7 to 1%, it can sustain compressive strains of up to 50% while maintaining its load-bearing capacity. Thus, when compressed beyond yield, the apparent modulus will reduce as a result of microcrack formation instead of individual trabeculae fracture. Upon repeated compressive loads events, trabecular bone tendentiously will lose stiffness and accumulate residual strain. Regarding trabecular tissue failure behavior, its ultimate yield strains are

higher in compression than in tension, and fatigue strength is lower than that of cortical bone. Trabecular bone is slightly viscoelastic, similarly to cortical bone [21,22,88,132–134].

Independently of being Haversian or trabecular, a bone's internal architecture and structure arrangement, and consequently its mechanical properties, are determined to a certain degree by adaptive mechanisms sensitive to their mechanical environment. This occurs through osteoclast's continuous removal of old bone—a process known as bone resorption—and its replacement with newly synthesized osteoid and its mineralization by osteoblasts—a process called ossification or bone formation—to form new bone. Bone remodeling is also present in the recovery process during injuries (e.g., fractures) in preventing future fractures by recovering daily activity-based microdamage in the bone tissue. Hence, cortical and trabecular bone mechanical properties will vary with the anatomic site (different bones from the same donor have demonstrated different mechanical properties), spatial positioning within the bones (e.g., between the epiphysis and diaphysis), disease (such as osteoarthritis), and age (balance between bone loss and gain is disrupted), which alter bone microstructure, loading direction, and loading mode [5,20,22,88,135].

6. Conclusions

Bone is a highly effective, natural composite presenting an exceptional combination of properties optimized by an evolutionary adaptive process to succeed in the surrounding environment. In this review, we showed how the unique mechanical properties of the bone are mainly caused by the hierarchical arrangement and the mechanical properties of different structures at different length scales. As highlighted in this article, bone structural characteristics and mechanical properties from different hierarchical levels influence its overall mechanical properties. Recent discoveries point towards the influence of the uniformity of mineral distribution and their interactions mainly on the bone elastic modulus as well as the balancing relation of the enzymatic and non-enzymatic collagen cross-linking in the reinforcement of bone strength and in the reduction in bone toughness and ultimate strain, respectively. This information will improve the development of bone–engineering nanocomposites, which not only need to mimic bone surface roughness and porosity, but also natural bone's nanostructure mechanical properties, in order to facilitate the propagation of osteoblasts and help in the regeneration of bones [136] and also in the field of bone adhesives [137]. Novel scientific investigations also demonstrated the relation between the physiological range of osteocyte lacunar porosity area, density, size, and orientation at the microscale level with the linear and the elastic modulus and ultimate bone strength. Accurate information regarding mechanical behavior at the macroscale as a response to the underlying microstructure properties and arrangement will improve the performance of bone-inspired metamaterial, for example, into the field of highly efficient construction materials [138] and in aerospace composite joints [139]. However, as emphasized by modern studies, there is an inseparable link between the structural organization and bone mechanical properties, where they are maintained by and adapted to the external mechanical stimulus, which consequently is influenced by the bone pericellular biomechanical and biophysical environment. Hence, the perception of bone as a living organ and how its hierarchical organization at different levels influences its properties is essential to understanding the relation between structure and functionality.

Synthetic composites have been developed intensively over the last few decades and have demonstrated an ascending application in a wide range of industries from civil infrastructures, transportations, aerospace, and even in the medical field. The high expectation placed on these materials created a need to innovate and to push the thinking beyond the conventional. Although the contemporary understanding and consensus on the concepts behind the structure–function relation have advanced enormously, the hierarchical complexity of bone structure, the extremely small scale involved in the lower hierarchical level, and the fact that, unlike the cases with engineering composites, isolating the different phases of bone tissue often involves a process that alters the properties being measured, increases the challenge associated with the study of bone at different length scales [21,22].

An in-depth comprehension of bone properties at different level scales, the interaction of the phases, as well as their variation among species, genders, ages, and anatomic sites will allow the successful translation of the principles into innovative composite technology. A better understanding, however, depends on future progress in research tools and technical approaches, such as new high-resolution imaging methods and compositional measurement techniques (e.g., quantitative three-dimensional microcomputed tomography, Raman microspectroscopy, backscattered electron imaging, and infrared spectroscopy), finite element modeling, nanotechnology (e.g., nanoindentation), acoustic microscopy, and histological and morphometric analysis. Improvements in the measurement techniques' reliability and resolution will allow for the development of more sophisticated and predictive numerical models (e.g., the inclusion of nano- and micro-features that highly influence macrostructure properties) and also their proper validation, which is now considered a limiting factor. Such knowledge will also serve as a model for the improvement of synthetic composites mimicking desirable features through the introduction of novel innovations in their structure, morphology, and mechanical properties or even to obtain materials with performances that were unimaginable in the past. These techniques will hopefully bring additional insights into this intricate composite and greatly contribute to synthetic composites' progress to satisfy the current and future demands of the engineering industry.

Author Contributions: Conceptualization, N.R., N.R. and M.F.S.F.M., investigation; original draft preparation, N.R. and M.F.S.F.M.; review and editing, S.O., R.S., F.D.M., A.T.M., J.P.S.F., A.R.R., M.C. and M.P.; supervision, R.S., F.D.M., A.T.M. and M.P.; project administration, A.T.M., S.O. and M.P.; funding acquisition, N.R., S.O. and M.P. All authors have read and agreed to the published version of the manuscript.

Funding: This research was funded by the European Union's Horizon 2020 research and innovation program, grant number 953169; by FCT/MEC (PIDDAC), project UIDB/50011/2020, UIDP/50011/2020, LA/P/0006/2020, LA/P/0045/2020 (ALiCE), UIDB/00511/2020 and UIDP/00511/2020 (LEPABE); by Foundation for Science and Technology (FCT), project UID/CTM/50025/2013, grant SFRH/BD/87089/2012, project UIDB/05256/2020, UIDP/0256/2020, project LAETA—UIDB/50022/2020 and UIDP/50022/2020.

Institutional Review Board Statement: Not applicable.

Informed Consent Statement: Not applicable.

Data Availability Statement: Not applicable.

Acknowledgments: This project was funded by the European Union's Horizon 2020 research and innovation program under grant agreement No 953169 in the scope of the InterLynk project. This work was also developed within the scope of the project CICECO-Aveiro Institute of Materials, UIDB/50011/2020, UIDP/50011/2020, LA/P/0006/2020, and projects LA/P/0045/2020 (ALiCE), UIDB/00511/2020 and UIDP/00511/2020 (LEPABE) financed by national funds through the FCT/MEC (PIDDAC). In addition, we acknowledge support from the Foundation for Science and Technology (FCT), Lisbon, Portugal, through Project UID/CTM/50025/2013, research grant SFRH/BD/87089/2012 (NR), project UIDB/05256/2020 and UIDP/0256/2020. We would also like to thank the support of FCT under the Project LAETA—UIDB/50022/2020.

Conflicts of Interest: The funders had no role in the design of the study; in the collection, analyses, or interpretation of data; in the writing of the manuscript, or in the decision to publish the results.

References

1. Adams, M.A. Functional anatomy of the musculoskeletal system. In *Gray's Anatomy: The Anatomical Basis of Clinical Practice*, 41st ed.; Standring, S., Ed.; Elsevier Health Sciences: London, UK, 2015; Volume 1, pp. 81–122.
2. Bonucci, E. Basic composition and structure of bone. In *Mechanical Testing of Bone and the Bone-Implant Interface*, 1st ed.; An, Y.H., Draughn, R.A., Eds.; CRC Press: Boca Raton, FL, USA, 2000; pp. 3–22.
3. Péoc'h, M. Normal histological architecture of tissue. In *Biomechanics and Biomaterials in Orthopedics*; Springer: London, UK, 2004; pp. 189–191.
4. Keller, T.S.; Liebschner, M.A. Tensile and Compression Testing of Bone. In *Mechanical Testing of Bone and the Bone-Implant Interface*, 1st ed.; An, Y.H., Draughn, R.A., Eds.; CRC Press: London, UK, 2000; pp. 175–206.

5. Rosa, N.; Simoes, R.; Magalhães, F.D.; Marques, A.T. From mechanical stimulus to bone formation: A review. *Med. Eng. Phys.* **2015**, *37*, 719–728. [CrossRef] [PubMed]
6. Koons, G.L.; Diba, M.; Mikos, A.G. Materials design for bone-tissue engineering. *Nat. Rev. Mater.* **2020**, *5*, 584–603. [CrossRef]
7. Bouchbinder, E.; Brener, E.A. Viscoelastic fracture of biological composites. *J. Mech. Phys. Solids* **2011**, *59*, 2279–2293. [CrossRef]
8. Libonati, F.; Vergani, L. Understanding the structure–property relationship in cortical bone to design a biomimetic composite. *Compos. Struct.* **2016**, *139*, 188–198. [CrossRef]
9. Ahn, T.; Gidley, D.W.; Thornton, A.W.; Wong-Foy, A.G.; Orr, B.G.; Kozloff, K.M.; Banaszak Holl, M.M. Hierarchical Nature of Nanoscale Porosity in Bone Revealed by Positron Annihilation Lifetime Spectroscopy. *ACS nano* **2021**, *15*, 4321–4334. [CrossRef]
10. Pai, S.; Kwon, J.; Liang, B.; Cho, H.; Soghrati, S. Finite element analysis of the impact of bone nanostructure on its piezoelectric response. *Biomech. Model. Mechanobiol.* **2021**, *20*, 1689–1708. [CrossRef]
11. Shekaran, A.; García, A.J. Extracellular matrix-mimetic adhesive biomaterials for bone repair. *J. Biomed. Mater. Res. A* **2011**, *96*, 261–272. [CrossRef]
12. Törnquist, E.; Gentile, L.; Prévost, S.; Diaz, A.; Olsson, U.; Isaksson, H. Comparison of small-angle neutron and X-ray scattering for studying cortical bone nanostructure. *Sci. Rep.* **2020**, *10*, 14552. [CrossRef]
13. Leo, L.; Bridelli, M.G.; Polverini, E. Reversible processes in collagen dehydration: A molecular dynamics study. *Arch. Biochem Biophys* **2021**, *714*, 109079. [CrossRef]
14. Gordon, M.K.; Hahn, R.A. Collagens. *Cell Tissue Res.* **2010**, *339*, 247–257. [CrossRef]
15. Hillgärtner, M.; Linka, K.; Itskov, M. Worm-like chain model extensions for highly stretched tropocollagen molecules. *J. Biomech.* **2018**, *80*, 129–135. [CrossRef] [PubMed]
16. Liu, Y.; Luo, D.; Wang, T. Hierarchical structures of bone and bioinspired bone tissue engineering. *Small* **2016**, *12*, 4611–4632. [CrossRef] [PubMed]
17. Friedrich, J. Analyzing Interactions between Cells and Extracellular Matrix by Atomic Force Microscopy. Ph.D. Thesis, Technischen Universität Dresden, Dresden, Germany, 2009.
18. Gültekin, O. *Computational Inelasticity of Fibrous Biological Tissues with a Focus on Viscoelasticity, Damage and Rupture*; Verlag der Technischen Universität Graz: Graz, Austria, 2019.
19. Van Gulick, L.; Saby, C.; Morjani, H.; Beljebbar, A. Age-related changes in molecular organization of type I collagen in tendon as probed by polarized SHG and Raman microspectroscopy. *Sci. Rep.* **2019**, *9*, 7280. [CrossRef] [PubMed]
20. Fonseca, J.E. Bone: A story of breakthroughs, a promising future. *Medicographia* **2012**, *34*, 142–148.
21. Keaveny, T.M.; Morgan, E.F.; Yeh, O.C. Bone mechanics. In *Standard Handbook of Biomedical Engineering & Design*, 1st ed.; Kutz, M., Ed.; McGraw-Hill: New York, NY, USA, 2003; pp. 200–222.
22. Morgan, E.F.; Barnes, G.L.; Einhorn, T.A. The bone organ system: Form and function. *Osteoporosis* **2008**, *1*, 3–25. [CrossRef]
23. Reznikov, N.; Bilton, M.; Lari, L.; Stevens, M.M.; Kröger, R. Fractal-like hierarchical organization of bone begins at the nanoscale. *Science* **2018**, *360*, eaao2189. [CrossRef]
24. Wang, Y.; Ural, A. A finite element study evaluating the influence of mineralization distribution and content on the tensile mechanical response of mineralized collagen fibril networks. *J. Mech. Behav. Biomed. Mater.* **2019**, *100*, 103361. [CrossRef]
25. Fratzl, P.; Gupta, H.S.; Paschalis, E.P.; Roschger, P. Structure and mechanical quality of the collagen–mineral nano-composite in bone. *J. Mater. Chem.* **2004**, *14*, 2115–2123. [CrossRef]
26. Chen, P.-Y.; Toroian, D.; Price, P.A.; McKittrick, J. Minerals form a continuum phase in mature cancellous bone. *Calcif. Tissue Int.* **2011**, *88*, 351–361. [CrossRef]
27. Zamiri, A.; De, S. Mechanical properties of hydroxyapatite single crystals from nanoindentation data. *J. Mech. Behav. Biomed. Mater.* **2011**, *4*, 146–152. [CrossRef]
28. White, T.D.; Black, M.T.; Folkens, P.A. *Human Osteology*, 3rd ed.; Academic Press: Oxford, UK, 2012.
29. Pang, S.; Schwarcz, H.P.; Jasiuk, I. Interfacial bonding between mineral platelets in bone and its effect on mechanical properties of bone. *J. Mech. Behav. Biomed. Mater.* **2021**, *113*, 104132. [CrossRef] [PubMed]
30. Barkaoui, A.; Hambli, R.; Tavares, J.M.R. Effect of material and structural factors on fracture behaviour of mineralised collagen microfibril using finite element simulation. *Comput. Methods Biomech. Biomed. Eng.* **2015**, *18*, 1181–1190. [CrossRef] [PubMed]
31. Trackman, P.C. Enzymatic and non-enzymatic functions of the lysyl oxidase family in bone. *Matrix Biol.* **2016**, *52*, 7–18. [CrossRef] [PubMed]
32. Garnero, P. The contribution of collagen crosslinks to bone strength. *BoneKEy Rep.* **2012**, *1*, 182. [CrossRef]
33. McNerny, E.M.; Gong, B.; Morris, M.D.; Kohn, D.H. Bone fracture toughness and strength correlate with collagen cross-link maturity in a dose-controlled lathyrism mouse model. *J. Bone Miner. Res.* **2015**, *30*, 455–464. [CrossRef]
34. Depalle, B.; Qin, Z.; Shefelbine, S.J.; Buehler, M.J. Influence of cross-link structure, density and mechanical properties in the mesoscale deformation mechanisms of collagen fibrils. *J. Mech. Behav. Biomed. Mater.* **2015**, *52*, 1–13. [CrossRef]
35. Banse, X.; Sims, T.; Bailey, A. Mechanical properties of adult vertebral cancellous bone: Correlation with collagen intermolecular cross-links. *J. Bone Miner. Res.* **2002**, *17*, 1621–1628. [CrossRef]
36. Siegmund, T.; Allen, M.R.; Burr, D.B. Failure of mineralized collagen fibrils: Modeling the role of collagen cross-linking. *J. Biomech.* **2008**, *41*, 1427–1435. [CrossRef]
37. Siegmund, T.; Allen, M.; Burr, D. A ductile-to-brittle transition in bone failure due to non-enzymatic collagen-crosslinks-A computational study. *Trans. Orthop. Res. Soc.* **2007**, *32*, 35.

38. Vashishth, D.; Wu, P.; Gibson, G. Age-related loss in bone toughness is explained by non-enzymatic glycation of collagen. *Trans. Orthop. Res. Soc.* **2004**, *29*, 497.
39. Allen, M.R.; Gineyts, E.; Leeming, D.J.; Burr, D.B.; Delmas, P.D. Bisphosphonates alter trabecular bone collagen cross-linking and isomerization in beagle dog vertebra. *Osteoporos. Int.* **2008**, *19*, 329–337. [CrossRef] [PubMed]
40. Ahn, A.C.; Grodzinsky, A.J. Relevance of collagen piezoelectricity to "Wolff's Law": A critical review. *Med. Eng. Phys.* **2009**, *31*, 733–741. [CrossRef] [PubMed]
41. Jilka, R.L.; Noble, B.; Weinstein, R.S. Osteocyte apoptosis. *Bone* **2013**, *54*, 264–271. [CrossRef] [PubMed]
42. Maghsoudi-Ganjeh, M.; Wang, X.; Zeng, X. Computational investigation of the effect of water on the nanomechanical behavior of bone. *J. Mech. Behav. Biomed. Mater.* **2020**, *101*, 103454. [CrossRef] [PubMed]
43. Masic, A.; Bertinetti, L.; Schuetz, R.; Chang, S.-W.; Metzger, T.H.; Buehler, M.J.; Fratzl, P. Osmotic pressure induced tensile forces in tendon collagen. *Nat. Commun.* **2015**, *6*, 5942. [CrossRef]
44. Keaveney, T.M. Cancellous bone. In *Handbook of Biomaterial Properties*; Black, J., Hastings, G., Eds.; Springer Science & Business Media: Dordrecht, The Netherlands, 2013; pp. 15–23.
45. Yoa, H. *Mechanical Testing of Bone and Bone-Like Materials Using Image Correlation Strain Measurement Technique*; Xi'an Jiaotong University: Xi'an, China, 2007.
46. Weld-Moore, R. *The Use of Quantitative Ultrasound to Investigate Bone Strength in the Facial Skeleton*; Trinity College: Dublin, Ireland, 2018.
47. Schwiedrzik, J.; Raghavan, R.; Bürki, A.; LeNader, V.; Wolfram, U.; Michler, J.; Zysset, P. In situ micropillar compression reveals superior strength and ductility but an absence of damage in lamellar bone. *Nat. Mater.* **2014**, *13*, 740–747. [CrossRef]
48. Doblaré, M.; García, J.M.; Gómez, M.J. Modelling bone tissue fracture and healing: A review. *Eng. Fract. Mech.* **2004**, *71*, 1809–1840. [CrossRef]
49. Arnett, T. *Osteocytes—Human Bone*; Bone Research Society: Peterborough, UK, 2015.
50. Arnett, T.; Manzano, J. *Osteoclast Resorption*; Bone Research Society: Peterborough, UK, 2015.
51. Mackenzie, K. *Osteocytes*; Bone Research Society: Peterborough, UK, 2015.
52. International Osteoporosis Foundation. Available online: https://www.osteoporosis.foundation/health-professionals/about-osteoporosis/bone-biology (accessed on 16 March 2022).
53. Kohli, N.; Ho, S.; Brown, S.J.; Sawadkar, P.; Sharma, V.; Snow, M.; García-Gareta, E. Bone remodelling in vitro: Where are we headed?—A review on the current understanding of physiological bone remodelling and inflammation and the strategies for testing biomaterials in vitro. *Bone* **2018**, *110*, 38–46. [CrossRef]
54. Moharrer, Y.; Boerckel, J.D. Tunnels in the rock: Dynamics of osteocyte morphogenesis. *Bone* **2021**, *153*, 116104. [CrossRef]
55. Kola, S.K.; Begonia, M.T.; Tiede-Lewis, L.M.; Laughrey, L.E.; Dallas, S.L.; Johnson, M.L.; Ganesh, T. Osteocyte lacunar strain determination using multiscale finite element analysis. *Bone Rep.* **2020**, *12*, 100277. [CrossRef]
56. Ramani-Mohan, R.-K.; Schwedhelm, I.; Finne-Wistrand, A.; Krug, M.; Schwarz, T.; Jakob, F.; Walles, H.; Hansmann, J. Deformation strain is the main physical driver for skeletal precursors to undergo osteogenesis in earlier stages of osteogenic cell maturation. *J. Tissue Eng Regen Med.* **2018**, *12*, e1474–e1479. [CrossRef] [PubMed]
57. Kameo, Y.; Ozasa, M.; Adachi, T. Computational framework for analyzing flow-induced strain on osteocyte as modulated by microenvironment. *J. Mech. Behav. Biomed. Mater.* **2022**, *126*, 105027. [CrossRef] [PubMed]
58. Mak, A.; Zhang, J. Numerical simulation of streaming potentials due to deformation-induced hierarchical flows in cortical bone. *J. Biomech. Eng.* **2001**, *123*, 66–70. [CrossRef] [PubMed]
59. Scheiner, S.; Pivonka, P.; Hellmich, C. Poromicromechanics reveals that physiological bone strains induce osteocyte-stimulating lacunar pressure. *Biomech. Model. Mechanobiol.* **2016**, *15*, 9–28. [CrossRef] [PubMed]
60. Zhao, F.; Garrigle, M.J.M.; Vaughan, T.J.; McNamara, L.M. In silico study of bone tissue regeneration in an idealised porous hydrogel scaffold using a mechano-regulation algorithm. *Biomech. Model. Mechanobiol.* **2018**, *17*, 5–18. [CrossRef] [PubMed]
61. Yu, K.; Sellman, D.P.; Bahraini, A.; Hagan, M.L.; Elsherbini, A.; Vanpelt, K.T.; Marshall, P.L.; Hamrick, M.W.; McNeil, A.; McNeil, P.L.; et al. Mechanical Loading Disrupts Osteocyte Plasma Membranes Which Initiates Mechanosensation Events in Bone. *J. Orthop. Res.* **2018**, *36*, 653–662. [CrossRef]
62. Burra, S.; Nicolella, D.P.; Francis, W.L.; Freitas, C.J.; Mueschke, N.J.; Poole, K.; Jiang, J.X. Dendritic processes of osteocytes are mechanotransducers that induce the opening of hemichannels. *Proc. Natl. Acad. Sci. USA* **2010**, *107*, 13648–13653. [CrossRef]
63. Spasic, M.; Jacobs, C.R. Lengthening primary cilia enhances cellular mechanosensitivity. *Eur. Cells Mater.* **2017**, *33*, 158–168. [CrossRef]
64. Hemmatian, H.; Bakker, A.D.; Klein-Nulend, J.; van Lenthe, G.H. Alterations in osteocyte lacunar morphology affect local bone tissue strains. *J. Mech. Behav. Biomed. Mater.* **2021**, *123*, 104730. [CrossRef]
65. Hamed, E.; Jasiuk, I. Multiscale damage and strength of lamellar bone modeled by cohesive finite elements. *J. Mech. Behav. Biomed. Mater.* **2013**, *28*, 94–110. [CrossRef]
66. Kaya, S.; Basta-Pljakic, J.; Seref-Ferlengez, Z.; Majeska, R.J.; Cardoso, L.; Bromage, T.G.; Zhang, Q.; Flach, C.R.; Mendelsohn, R.; Yakar, S. Lactation-induced changes in the volume of osteocyte lacunar-canalicular space alter mechanical properties in cortical bone tissue. *J. Bone Miner. Res.* **2017**, *32*, 688–697. [CrossRef] [PubMed]
67. Sang, W.; Li, Y.; Guignon, J.; Liu, X.S.; Ural, A. Structural role of osteocyte lacunae on mechanical properties of bone matrix: A cohesive finite element study. *J. Mech. Behav. Biomed. Mater.* **2022**, *125*, 104943. [CrossRef] [PubMed]

68. Burr, D.B. Stress concentrations and bone microdamage: John Currey's contributions to understanding the initiation and arrest of cracks in bone. *Bone* **2019**, *127*, 517–525. [CrossRef] [PubMed]
69. Josephson, T.O.; Moore, J.P.; Maghami, E.; Freeman, T.A.; Najafi, A.R. Computational study of the mechanical influence of lacunae and perilacunar zones in cortical bone microcracking. *J. Mech. Behav. Biomed. Mater.* **2021**, *126*, 105029. [CrossRef]
70. Uda, Y.; Azab, E.; Sun, N.; Shi, C.; Pajevic, P.D. Osteocyte Mechanobiology. *Curr. Osteoporos. Rep.* **2017**, *15*, 318–325. [CrossRef]
71. Dallas, S.L.; Prideaux, M.; Bonewald, L.F. The osteocyte: An endocrine cell . . . and more. *Endocr. Rev.* **2013**, *34*, 658–690. [CrossRef]
72. Lemaire, T.; Capiez-Lernout, E.; Kaiser, J.; Naili, S.; Rohan, E.; Sansalone, V. A multiscale theoretical investigation of electric measurements in living bone. *Bull. Math. Biol.* **2011**, *73*, 2649–2677. [CrossRef]
73. Bonewald, L.F. The amazing osteocyte. *J. Bone Miner. Res.* **2011**, *26*, 229–238. [CrossRef]
74. Dutta, S.K.; Datta, D. Composition of musculoskeletal structures. In *Applied Orthopaedic Biomechanics*, 1st ed.; Dutta, S.K., Datta, D., Eds.; BI Publications Pvt Ltd.: New Delhi, India, 2008; pp. 29–37.
75. Mckibbin, B. The biology of fracture healing in long bones. *J. Bone Jt. Surg. Br.* **1978**, *60-B*, 150–162. [CrossRef]
76. Cartmell, S.; Rupani, A.; Balint, R. Osteoblasts and their applications in bone tissue engineering. *Cell Health Cytoskelet.* **2012**, *49*, 49–61. [CrossRef]
77. Aarden, E.M.; Nijweide, P.J.; Burger, E.H. Function of osteocytes in bone. *J. Cell. Biochem.* **1994**, *55*, 287–299. [CrossRef] [PubMed]
78. George, D.; Allena, R.; Remond, Y. Integrating molecular and cellular kinetics into a coupled continuum mechanobiological stimulus for bone reconstruction. *Contin. Mech. Thermodyn.* **2019**, *31*, 725–740. [CrossRef]
79. Martin, M.; Sansalone, V.; Cooper, D.M.; Forwood, M.R.; Pivonka, P. Mechanobiological osteocyte feedback drives mechanostat regulation of bone in a multiscale computational model. *Biomech. Model. Mechanobiol.* **2019**, *18*, 1475–1496. [CrossRef] [PubMed]
80. Zhang, X.; Wang, H.; Hao, Z. A numerical bone regeneration model incorporating angiogenesis, considering oxygen-induced secretion of vascular endothelial growth factor and vascular remodeling. *J. Biomech.* **2021**, *127*, 110656. [CrossRef]
81. Peyroteo, M.; Belinha, J.; Natal Jorge, R. Load adaptation through bone remodeling: A mechanobiological model coupled with the finite element method. *Biomech. Model. Mechanobiol.* **2021**, *20*, 1495–1507. [CrossRef]
82. Isaksson, H. Recent advances in mechanobiological modeling of bone regeneration. *Mech. Res. Commun.* **2012**, *42*, 22–31. [CrossRef]
83. Ascenzi, M.-G.; Kawas, N.P.; Lutz, A.; Kardas, D.; Nackenhorst, U.; Keyak, J.H. Individual-specific multi-scale finite element simulation of cortical bone of human proximal femur. *J. Comput. Phys.* **2013**, *244*, 298–311. [CrossRef]
84. Morgan, E.F.; Keaveny, T.M. Dependence of yield strain of human trabecular bone on anatomic site. *J. Biomech.* **2001**, *34*, 569–577. [CrossRef]
85. McCalden, R.W.; McGeough, J.A.; Barker, M.B. Age-related changes in the tensile properties of cortical bone. The relative importance of changes in porosity, mineralization, and microstructure. *J. Bone Jt. Surg. Am.* **1993**, *75*, 1193–1205. [CrossRef]
86. Cowin, S.C. Bone poroelasticity. *J. Biomech.* **1999**, *32*, 217–238. [CrossRef]
87. Weinbaum, S.; Cowin, S.C.; Zeng, Y. A model for the excitation of osteocytes by mechanical loading-induced bone fluid shear stresses. *J. Biomech.* **1994**, *27*, 339–360. [CrossRef]
88. Shore, S.W.; Unnikrishnan, G.U.; Hussein, A.I.; Morgan, E.F. Bone biomechanics. In *Orthopaedic Biomechanics*; Winkelstein, B.A., Ed.; CRC Press: Boca Raton, FL, USA, 2013; pp. 3–47.
89. Porteous, M.; Bäuerle, S. *Techniques and Principles for the Operating Room*; Georg Thieme Verlag: Stuttgart, Germany, 2010.
90. Dutta, S.K.; Datta, D. Long bone shape its mechanical significance. In *Applied Orthopaedic Biomechanics*, 1st ed.; Dutta, S.K., Datta, D., Eds.; BI Publications Pvt Ltd.: New Delhi, India, 2008; pp. 41–49.
91. Taddei, F.; Cristofolini, L.; Martelli, S.; Gill, H.S.; Viceconti, M. Subject-specific finite element models of long bones: An in vitro evaluation of the overall accuracy. *J. Biomech.* **2006**, *39*, 2457–2467. [CrossRef] [PubMed]
92. Papini, M.; Zdero, R.; Schemitsch, E.H.; Zalzal, P. The biomechanics of human femurs in axial and torsional loading: Comparison of finite element analysis, human cadaveric femurs, and synthetic femurs. *J. Biomech. Eng.* **2007**, *129*, 12–19. [CrossRef] [PubMed]
93. Hench, L.L.; Wilson, J. Introduction. In *An Introduction to Bioceramics*; World Scientific: Singapore, 1993; pp. 1–24.
94. Currey, J. Cortical bone. In *Handbook of Biomaterial Properties*, 1st ed.; Black, J., Hastings, G., Eds.; Springer Science & Business Media: London, UK, 1998; Volume I, pp. 3–13.
95. Morawska-Chochół, A.; Chłopek, J.; Szaraniec, B.; Domalik-Pyzik, P.; Balacha, E.; Boguń, M.; Kucharski, R. Influence of the intramedullary nail preparation method on nail's mechanical properties and degradation rate. *Mater. Sci. Eng. C* **2015**, *51*, 99–106. [CrossRef] [PubMed]
96. Ramakrishna, S.; Mayer, J.; Wintermantel, E.; Leong, K.W. Biomedical applications of polymer-composite materials: A review. *Compos. Sci. Technol.* **2001**, *61*, 1189–1224. [CrossRef]
97. Byrne, D.P.; Lacroix, D.; Prendergast, P.J. Simulation of fracture healing in the tibia: Mechanoregulation of cell activity using a lattice modeling approach. *J. Orthop. Res.* **2011**, *29*, 1496–1503. [CrossRef]
98. Wang, X.; Nyman, J.S.; Dong, X.; Leng, H.; Reyes, M. *Fundamental Biomechanics in Bone Tissue Engineering*; Morgan & Claypool: San Rafael, CA, USA, 2010.
99. Neto, R.B.; Rossi, J.D.M.B.A.; Leivas, T.P. Experimental determination of bone cortex holding power of orthopedic screw. *Rev. Hosp. Clin. Fac. Med. Sao Paulo* **1999**, *54*, 181–186. [CrossRef]
100. Drake, R.L.; Vogl, A.W.; Mitchell, A.W.M. *Gray's Basic Anatomy*, 2nd ed.; Elsevier Health Sciences: Amsterdam, The Netherlands, 2016; pp. 265–340.

101. Munford, M.J.; Ng, K.G.; Jeffers, J.R. Mapping the multi-directional mechanical properties of bone in the proximal tibia. *Adv. Funct. Mater.* **2020**, *30*, 2004323. [CrossRef]
102. Hashemi, J.; Chandrashekar, N.; Gill, B.; Beynnon, B.D.; Slauterbeck, J.R.; Schutt, R.t.C.; Mansouri, H.; Dabezies, E. The geometry of the tibial plateau and its influence on the biomechanics of the tibiofemoral joint. *J. Bone Jt. Surg. Am.* **2008**, *90*, 2724–2734. [CrossRef]
103. Hurwitz, D.E.; Sumner, D.R.; Andriacchi, T.P.; Sugar, D.A. Dynamic knee loads during gait predict proximal tibial bone distribution. *J. Biomech.* **1998**, *31*, 423–430. [CrossRef]
104. Lu, T.-W.; O'Connor, J.J.; Taylor, S.J.G.; Walker, P.S. Validation of a lower limb model with in vivo femoral forces telemetered from two subjects. *J. Biomech.* **1997**, *31*, 63–69. [CrossRef]
105. Lu, T.-W.; O'Connor, J.J.; Taylor, S.J.G.; Walker, P.S. Comparison of telemetered femoral forces with model calculations. *J. Biomech.* **1998**, *31*, 47. [CrossRef]
106. Taylor, S.J.G.; Walker, P.S.; Perry, J.S.; Cannon, F.R.C.S.; Woledge, R. The forces in the distal femur and the knee during walking and other activities measured by telemetry. *J. Arthroplast.* **1998**, *13*, 428–437. [CrossRef]
107. Taylor, S.J.G.; Walker, P.S. Forces and moments telemetered from two distal femoral replacements during various activities. *J. Biomech.* **2001**, *34*, 839–848. [CrossRef]
108. Wehner, T.; Claes, L.; Simon, U. Internal loads in the human tibia during gait. *Clin. Biomech.* **2009**, *24*, 299–302. [CrossRef]
109. Taylor, W.R.; Heller, M.O.; Bergmann, G.; Duda, G.N. Tibio-femoral loading during human gait and stair climbing. *J. Orthop. Res.* **2004**, *22*, 625–632. [CrossRef]
110. Nagura, T.; Matsumoto, H.; Kiriyama, Y.; Chaudhari, A.; Andriacchi, T.P. Tibiofemoral joint contact force in deep knee flexion and its consideration in knee osteoarthritis and joint replacement. *J. Appl. Biomech.* **2006**, *22*, 305–313. [CrossRef]
111. D'Lima, D.D.; Townsend, C.P.; Arms, S.W.; Morris, B.A.; Colwell, C.W., Jr. An implantable telemetry device to measure intra-articular tibial forces. *J. Biomech.* **2005**, *38*, 299–304. [CrossRef]
112. Zhao, D.; Banks, S.A.; D'Lima, D.D.; Colwell, C.W.; Fregly, B.J. In vivo medial and lateral tibial loads during dynamic and high flexion activities. *J. Orthop. Res.* **2007**, *25*, 593–602. [CrossRef]
113. Kim, H.J.; Fernandez, J.W.; Akbarshahi, M.; Walter, J.P.; Fregly, B.J.; Pandy, M.G. Evaluation of predicted knee-joint muscle forces during gait using an instrumented knee implant. *J. Orthop. Res.* **2009**, *27*, 1326–1331. [CrossRef]
114. D'Angeli, V.; Belvedere, C.; Ortolani, M.; Giannini, S.; Leardini, A. Load along the tibial shaft during activities of daily living. *J. Biomech.* **2014**, *47*, 1198–1205. [CrossRef] [PubMed]
115. Ellis, M.I.; Seedhom, B.B.; Wright, V. Forces in the knee joint whilst rising from a seated position. *J. Biomed. Eng.* **1984**, *6*, 113–120. [CrossRef]
116. Wilk, K.E.; Escamilla, R.F.; Fleisig, G.S.; Barrentine, S.W.; Andrews, J.R.; Boyd, M.L. A comparison of tibiofemoral joint forces and electromyographic activity during open and closed kinetic chain exercises. *Am. J. Sports Med.* **1996**, *24*, 518–527. [CrossRef] [PubMed]
117. Dahlkvist, N.J.; Mayo, P.; Seedhom, B.B. Forces during squatting and rising from a deep squat. *Eng. Med.* **1982**, *11*, 69–76. [CrossRef]
118. Norman, T.L.; Vashishtht, D.; Burr, D.B. Fracture toughness of human bone under tension. *J. Biomech.* **1995**, *28*, 309–320. [CrossRef]
119. Phelps, J.B.; Hubbard, G.B.; Wang, X.; Agrawal, C.M. Microstructural heterogeneity and the fracture toughness of bone. *J. Biomed. Mater. Res. A* **2000**, *51*, 735–741. [CrossRef]
120. Morais, J.J.L.; de Moura, M.F.S.F.; Pereira, F.A.M.; Xavier, J.; Dourado, N.; Dias, M.I.R. The double cantilever beam test applied to mode I fracture characterization of cortical bone tissue. *J. Mech. Behav. Biomed.* **2010**, *3*, 446–453. [CrossRef]
121. Norman, T.L.; Nivargikar, V.; Burr, D.B. Resistance to crack growth in human cortical bone is greater in shear than in tension. *J. Biomech.* **1996**, *29*, 1023–1031. [CrossRef]
122. Dourado, N.; Pereira, F.A.M.; de Moura, M.F.S.F.; Morais, J.J.L.; Dias, M.I.R. Bone fracture characterization using the end notched flexure test. *Mater. Sci. Eng. C* **2013**, *33*, 405–410. [CrossRef]
123. Zimmermann, E.A.; Launey, M.E.; Ritchie, R.O. The significance of crack-resistance curves to the mixed-mode fracture toughness of human cortical bone. *Biomaterials* **2010**, *31*, 5297–5305. [CrossRef]
124. Pereira, F.A.M.; de Moura, M.F.S.F.; Dourado, N.; Morais, J.J.L.; Dias, M.I.R. Bone fracture characterization under mixed-mode I+II loading using the single leg bending test. *Biomech. Model. Mechanobiol.* **2014**, *13*, 1331–1339. [CrossRef] [PubMed]
125. Pereira, F.A.M.; de Moura, M.F.S.F.; Dourado, N.; Morais, J.J.L.; Silva, F.G.A.; Dias, M.I.R. Bone fracture characterization under mixed-mode I+II loading using the MMB test. *Eng. Fract. Mech.* **2016**, *166*, 151–163. [CrossRef]
126. Wang, X.; Puram, S. The toughness of cortical bone and its relationship with age. *Ann. Biomed. Eng.* **2004**, *32*, 123–135. [CrossRef]
127. Yang, Q.D.; Cox, B.N.; Nalla, R.K.; Ritchie, R.O. Fractur.re length scales in human cortical bone: The necessity of non-linear fracture models. *Biomaterials* **2006**, *27*, 2095–2113. [CrossRef] [PubMed]
128. An, Y.H.; Barfield, W.R.; Draughn, R.A. Basic concepts of mechanical property measurement and bone biomechanics. In *Mechanical Testing of Bone and the Bone-Implant Interface*, 1st ed.; An, Y.H., Draughn, R.A., Eds.; CRC Press: Boca Raton, FL, USA, 2000; pp. 23–40.
129. Arnold, P.A. Validation of Mechanical Response Tissue Analysis by Three-Point Mechanical Bending of Artificial Human Ulnas. Bachelor's Thesis, Ohio University, Athens, OH, USA, 2013.

130. Carnelli, D. Orientation and Length-Scale Dependent Mechanical Properties in Lamellar Bone at the Micro and Nanostructural Hierarchical Levels. Politecnico di Milano, Milan, Italy, 2010.
131. Colabella, L.; Cisilino, A.P.; Häiat, G.; Kowalczyk, P. Mimetization of the elastic properties of cancellous bone via a parameterized cellular material. *Biomech. Model. Mechanobiol.* **2017**, *16*, 1485–1502. [CrossRef] [PubMed]
132. Keaveny, T.M. Cancellous bone. In *Handbook of Biomaterial Properties*, 1st ed.; Black, J., Hastings, G., Eds.; Springer Science & Business Media: London, UK, 1998; Volume I, pp. 15–23.
133. Parkinson, H.; Fazzalari, N.L. Characterisation of trabecular bone structure. In *Skeletal Aging and Osteoporosis*, 1st ed.; Silva, M.J., Gefen, A., Aviv, R., Eds.; Studies in Mechanobiology, Tissue Engineering and Biomaterials; Springer: London, UK, 2013; pp. 31–51.
134. Rahmoun, J.; Chaari, F.; Markiewicz, E.; Drazetic, P. Micromechanical modeling of the anisotropy of elastic biological composites. *Multiscale Model. Simul.* **2009**, *8*, 326–336. [CrossRef]
135. Kini, U.; Nandeesh, B.N. *Physiology of bone formation, remodeling, and metabolism In Radionuclide and Hybrid. Bone Imaging*, 1st ed.; Fogelman, I., Gnanasegaran, G., van der Wall, H., Eds.; Springer: Berlin/Heidelberg, Germany, 2012; pp. 29–57.
136. Zhu, L.; Luo, D.; Liu, Y. Effect of the nano/microscale structure of biomaterial scaffolds on bone regeneration. *Int. J. Oral Sci.* **2020**, *12*, 6. [CrossRef]
137. Park, S.B.; Sung, M.H.; Uyama, H.; Han, D.K. Poly (glutamic acid): Production, composites, and medical applications of the next-generation biopolymer. *Prog. Polym. Sci.* **2021**, *113*, 101341. [CrossRef]
138. Naboni, R.; Kunic, A. Bone-inspired 3D printed structures for construction applications. *Gestão Tecnol. Proj.* **2019**, *14*, 111–124. [CrossRef]
139. Burns, L. Bio-Inspired Design of Aerospace Composite Joints. Ph.D. Thesis, RMIT University, Melbourne, Australia, 2012.